Anti-Kasha Conformational Photo-isomerization of a Heteroleptic Dithiolene Metal Complex Revealed by Ultrafast Spectroscopy

Michela Gazzetto,[a] Flavia Artizzu,[b] Salahuddin S. Attar,[c,#] Luciano Marchiò,[d] Luca Pilia,[e] Egmont J. Rohwer,[a] Thomas Feurer,[a] Paola Deplano,[c] Andrea Cannizzo*[a]*

[a] Institute of Applied Physics, University of Bern, Sidlerstrasse 5, 3012 Bern (Switzerland)

[b] L3-Luminescent Lanthanide Lab, Department of Chemistry, Ghent University, Krijgslaan 281-building S3, B-9000, Gent (Belgium).

[c] Department of Chemical and Soil Sciences, University of Cagliari, 09042, Monserrato (CA) (Italy).

[d] Dipartimento di Scienze Chimiche, della Vita e della Sostenibilità Ambientale, Università di Parma, Parco Area delle Scienze 17/a, 43124, Parma (Italy)

[e] Dipartimento di Ingegneria Meccanica, Chimica e dei Materiali, Università di Cagliari, Via Marengo 2, 09123, Cagliari (Italy).

Currently at the Department of Chemistry, Texas A&M University at Qatar, Texas A&M Engineering Building, Education City, Doha, (Qatar).

*corresponding authors: andrea.cannizzo@iap.unibe.ch, deplano@unica.it.

ABSTRACT. We investigated the anti-Kasha photochemistry and anti-Kasha emission of a d^8-metal donor-acceptor dithiolene with femtosecond UV-Vis transient absorption spectroscopy and molecular modeling. Experimentally, we found a lifetime of 1.4 ps for the higher excited states, which is exceptionally long when compared to typical values for internal conversion (10s of fs or less). Consequently, a substantial emission originates from the second excited state. Molecular modeling suggests this to be a consequence of the spatially separated molecular orbitals of first and second excited states, which gives a charge transfer character to the internal conversion. More surprisingly, we found that the inherent flexibility of the molecule allows the metal complex to access different configurations depending on the photo-excited state. We believe that this unique manifestation of anti-Kasha conformational photo-isomerization is facilitated by the exceptionally long lifetime of the second excited state.

TOC GRAPHICS

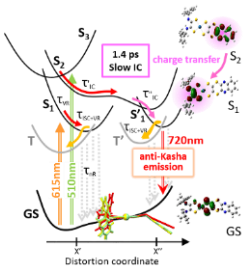

KEYWORDS. Dithiolene, Metal complexes, anti-Kasha photochemistry, anti-Kasha emission, photocycle, ultrafast spectroscopy.

TEXT. Kasha's rule is a fundamental empirical principle of photophysics and photochemistry, connecting excitation and emission processes.[1,2] Few cases of its violation are nowadays known,[3–5] and they have proven to be extremely interesting for applications as multiresponsive photo-active materials,[6,7] dual-emission probes,[8,9] or to achieve a more efficient utilization of the photo-absorbed energy.[10,11] Moreover, the study of molecular systems showing an anti-Kasha behavior can allow the study of the relaxation mechanisms and molecular processes on or from higher excited-states, with an evident benefit in terms of comprehension of fundamental molecular physics and improvement of computational quantum chemistry tools.[12–14]

Recently, novel platinum dithiolene complexes, both homo-and hetero-leptic, with Quinoxdt (= [4',5':5,6][1,4]dithiino[2,3-b]quinoxaline-1',3'dithiolato)[15–17] have shown a peculiar anti-Kasha behavior displaying photoluminescence only upon excitation of the higher electronic states, and no emission when exciting in the lowest electronic absorption band.[1] In heteroleptic d^8-metal dithiolene complexes (Figure S1) fine modulation of ligands affords planar and low-energy-gap chromophores consisting of a π-acceptor (A) and a π-donor (D) ligand connected in a square-planar coordination by the metal, working as a suitable dπ-bridge for the D-A charge transfer (CT) transition. This unique system allows for remarkable linear and nonlinear optical properties[18,19] among which, with the choice of the suitable ligands, also a multiresponsive behavior due to an anti-Kasha response.[15]

Scheme 1. Structural formula of Bu_4N[Pt(MBAdto)(Quinoxdt)]. The donor ligands and the acceptor ligand are highlighted in red and blue, respectively.

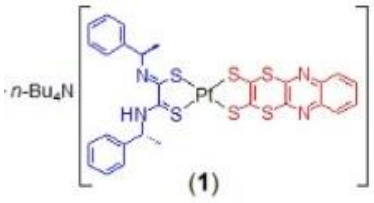

In the case of the anionic complex $[Pt(MBAdto)(Quinoxdt)]^-$ [(**1**), Scheme 1], where the acceptor ligand is (R)-(+)-α-Methyl benzyl dithio-oxamidate [MBAdto], the observed anti-Kasha behavior was tentatively attributed to a poor spatial overlap between the emissive state, mainly centered on the quinoxaline moiety (LUMO+1), and the lower energy state, mainly related to the MBAdto moiety (LUMO).[15,16] The internal conversion (IC) between these two states is therefore characterized by a strong ligand-to-ligand charge transfer (CT) character. This condition should slow down the IC process to ~10 ps,[15] making the radiative decay detectable. This is exceptionally long for a higher excited state and requires a direct validation. Therefore, ultrafast transient absorption (TA) upon excitation of different excited states is employed to clarify the origin of the anti-Kasha behavior in platinum-complexes bearing the Quinoxdt ligand. TA reveals the relevant time scales of the involved processes and allows to establish the photocycle of (**1**) as a representative example of this class of Pt-dithiolenes.

The electronic optical absorption (OA) of complex (**1**) (Figure 1a) shows a visible band at 595 nm in CH_3CN with a shoulder at ~500 nm.[15] Upon irradiation in the range 420-520 nm (**1**) it shows photoluminescence at λ = 720 nm at room temperature (Φ=6.4x10^{-5}). Figure 1b displays the

molecular orbitals (MOs) involved in the absorption transition. According to density functional theory (DFT) and time-dependent (TD)-DFT calculations (see Figure S2 and related discussion), the lowest frequency absorption is assigned to a HOMO → LUMO transition into the lowest singlet excited state (S_1) corresponding to an electron transfer from the mixed Quinoxdt ligand and metal moiety to the MBAdto ligand.[15] The shoulder at 500 nm is dominated by two HOMO → LUMO+1 and HOMO-1 → LUMO transitions to the second (S_2) and third (S_3) singlet excited states, respectively, (Figure S2, Figure S3, Table S2). Emissions (Table S3 and related discussion) from equilibrated S_1 and S_2 to the non-equilibrium ground state (GS) are centered at 872 nm and 673 nm, respectively, and originate from a LUMO → HOMO and LUMO+1 → HOMO transitions, respectively. The comparison of the optimized molecular geometries of the GS, S_1 and S_2 states (Figure S4) reveals that the system undergoes significant conformational changes upon relaxation from S_2 to S_1 and then to GS.

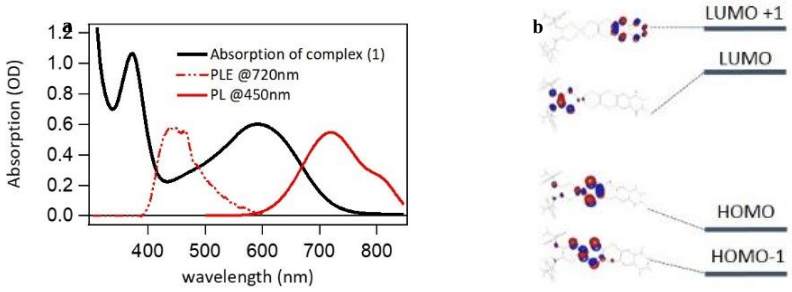

Figure 1. **a**, Optical absorption spectra, excitation spectrum (PLE) monitoring 720 nm emission and emission spectrum (PL) upon 450 nm excitation of (**1**) in CH_3CN. **b**, Molecular orbitals (MOs) involved in these optical transitions (see figure S3 for a more extended set of MOs).

The ultrafast dynamics in and from higher excited states upon 510 nm excitation, is investigated in comparison to the excitation to S_1 at 615 nm to unveil the origin of the anti-Kasha 720 nm

emission. Excitation at 615 nm allows an efficient population transfer to the lowest excited state without inducing anti-Kasha emission (see excitation spectrum, PLE, in Figure 1a). Conversely, the 510 nm excitation is the shortest wavelength that results in an anti-Kasha emission PLE spectrum.

The observed dynamics of (**1)** upon excitation at 615 nm (Figure 2a and 2b) provides a simple photophysical picture (see section S5 of the SI for a more detailed discussion). After photoexcitation of the S_1 state, the system undergoes first vibrational relaxation (VR) in 220 fs and later inter-system crossing (ISC) to low-lying triplet states (T_1) in 7 ps, accompanied by non-radiative relaxation to the GS. The relaxed T_1 state is long lived and the only further dynamics observed is ascribed to a rotational diffusion in 176 ps (see Table 1). The proposed photocycle is corroborated by a previous ultrafast study on a closely related class of d^8-metal D-M-A heteroleptic-dithiolene complexes, where a $S_1 \rightarrow T_1$ ISC process with the same rate was reported.[20] The left side of Figure 3 shows the photocycle upon GS$\rightarrow S_1$ excitation (see also Figure S11a).

Table 1. Kinetic parameters determined by SVD analysis of TA spectra measured in acetonitrile at different excitation wavelengths.

Excitation (nm)	τ'_{IC} (ps)	τ''_{IC} (ps)	τ_{VR} (ps)	τ_{ISC+VR} (ps)	τ_{ROT} (ps)	τ_T (ps)
615	-	-	0.22± 0.03	7.0± 0.1	174± 13	∞
510	0.15± 0.015	1.4 ± 0.5	-	5.7 ± 0.5	196± 11	∞

Notation for time constant labels: IC: internal conversion, VR: vibrational relaxation, ISC: intersystem crossing, Rot: rotation, T: triplet state.

When tuning the excitation to 510 nm, the TA spectra are very similar to those at 615 nm excitation (Figure 2c and 2a, respectively), revealing that, regardless of the excitation wavelength, the TA spectra are mainly representative of the dynamics and population of S_1 first and T_1 later. Despite this strong similarity, their spectral evolution shows several important differences, which can be better identified through the decay associated spectra (DAS) obtained via singular value decomposition (SVD) (Figure 2d and Figure S10). We find that the dynamics is fully described by five DASs with time constants 150 fs, 1.4 ps, 5.7 ps, 196 ps and ∞ (Table 1). The first two DASs have a similar shape and describe a rise of the ESA band at 435 nm and decay of a broad ESA band at λ>500 nm with 150 fs and 1.4 ps time constants. These are not observed upon direct excitation of S_1 and at later times the TA spectrum and DASs become very similar to the ones upon 615 nm irradiation (Figure 2). Consequently, we can safely assign these contributions to a biphasic IC from higher excited states towards S_1 population. Accordingly, the last three components (τ_3 = 5.7 ± 0.5 ps, τ_4 = 196 ± 11 ps and τ_5=∞) can be assigned to the respective last three components upon 615 nm excitation: ISC from S_1 to the low-lying triplet states, rotational diffusion and long-lived triplet state, respectively. These assignments are definitively validated by substantial equivalence of the respective time constants (Table 1).

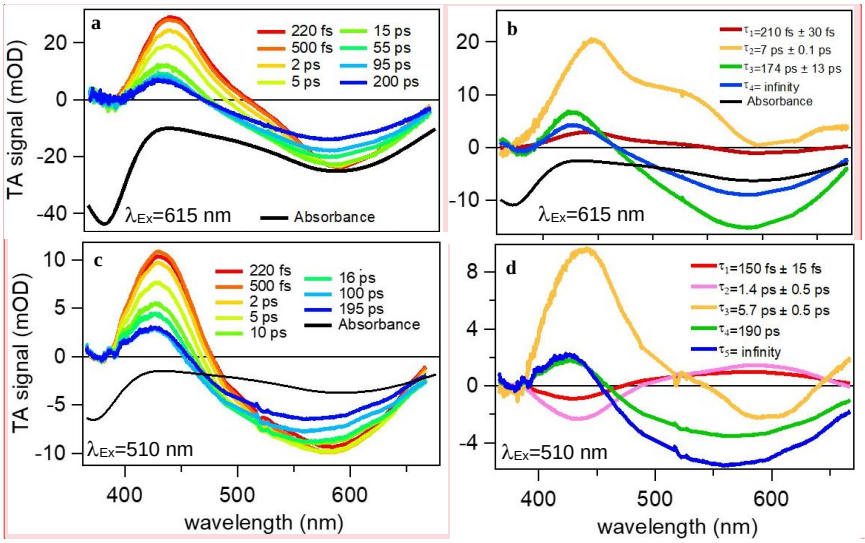

Figure 2. Representative selection of TA spectra at different time delays in acetonitrile upon 615 nm (**a**) and 510 nm (**c**) excitation, extracted from 2D TA time-wavelength experiment (Figure S5 and Figure S9). The black curve shows the inverted ground-state absorption spectrum. DAS obtained by SVD analysis of the TA experimental matrix upon 615 nm (**b**) and upon 510 nm (**d**) excitation, respectively. Each curve is labeled with the respective time constant. $\tau = \infty$ describes a contribution with a dynamics much longer than the scanned interval and is modeled with a step function.

An IC process in 1.4 ps is exceptionally long when compared to tens of fs, which are more typical timescales for such a process.[21] To rationalize such an exceptionally long IC process and multi-exponential behavior, we consider first the involved electron spatial density distributions of the different excited states. According to Figure 1b and Table S2 the IC process $S_2 \rightarrow S_1$ corresponds to a non-radiative LUMO+1→LUMO transition, while $S_3 \rightarrow S_1$ would be a non-radiative

Commentato [MG1]: Check picture resolution

HOMO→HOMO-1 transition. In the former, there is no spatial overlap between the involved MOs and the IC process is *de facto* a long-range radiationless CT process. This condition could dramatically slow down the IC process even to ps time scales. Conversely, HOMO-1 and HOMO have a strong overlap and the $S_3 \rightarrow S_1$ IC is not accompanied by an important reorganization of the electrons around and in the molecule. However, this favorable condition could be partially balanced by the wide S_3-S_1 energy gap (energy gap law)[22], and a timescale of a few 100s of fs could be reasonable. Regarding the $S_3 \rightarrow S_2$ IC process, this is accompanied by charge reorganization similar to $S_2 \rightarrow S_1$, but speeded up by a smaller energy gap, suggesting a value of the IC rate between the $S_3 \rightarrow S_1$ and $S_2 \rightarrow S_1$ IC rates. However, this line of reasoning should not be pushed too much further and should be considered as a qualitative approach to estimate the efficiency of a given IC relaxation path. Specifically, it allows us to rationalize the presence of an unusually long IC process because of its CT character and therefore to assign the 1.4 ps DAS to the $S_2 \rightarrow S_1$ IC process and the fast 150 fs DAS to the competition between $S_3 \rightarrow S_1$ and $S_3 \rightarrow S_2$. For the sake of completeness, we compare in the SI these direct estimations of IC rates with the indirect ones from literature (section S10).

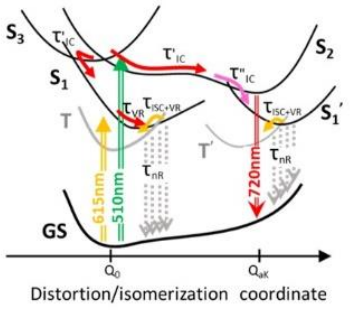

Figure 3. Photocycle of (**1**) upon 615 nm excitation into the lowest S_1 excited state and upon 510 nm excitation into higher excited states (S_2 and S_3). The anti-Kasha photo-isomerization is explicitly depicted, as a function of a generalized isomerization coordinate. Arrows representing individual relaxation steps are color-coded according to the respective DASs in Figure 6B and D. See Table 1 for the time constant values and notation. Electronic states nomenclature: GS, ground state; S_n, nth singlet excited state; T, low-lying triplet states; S_1', and T' electronic states in the equilibrium configuration of the anti-Kasha conformer (Q_{aK}).

According to the previous discussion, after IC and after ISC (see photocycle in Figure S11b), the system should be found in S_1 and T, respectively. We could initially observe small differences, due to the different thermal state but, after few ps, we should observe the same TA spectra and DASs, regardless of the excitation wavelength. This is only partially true as exemplified by Figure 4 where the long-lived components are compared. A major difference is observed in the range 480-600 nm (Figure 4), where an ESA band at 510 nm is missing or strongly reduced, as highlighted by the differential spectrum. The lack of this band at any time (Figure S12), in any relaxation process (Figure S13) and especially in the longest times spectra (Figure 4) strongly points to a long-lived distortion dependent on the initial excited state. Its origin can be

conformational or electronic, however, since all the main spectral features are preserved, we are in favor of a conformational distortion. The comparison of the optimized geometries of *GS*, S_1 and S_2 states (Figure S4) supports this, confirming that the molecule undergoes important and global conformational changes upon inter-state transitions. It also suggests that the molecule is not rigid but is prone to exploring different geometries during the relaxation. Interestingly, the molecular geometry of *GS* is very similar to that of S_2 but it is significantly different from that of S_1.

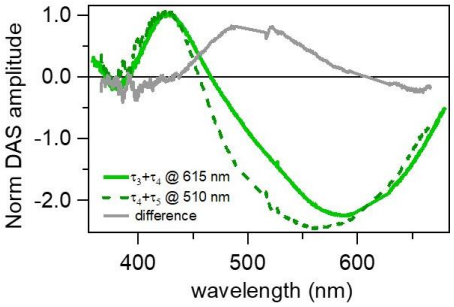

Figure 4. Comparison between the sum of the last DASs from Figure 2b and d. For sake of comparison, data are normalized to the maximum. Solid and dashed lines refer to 615 nm and 510 nm excitation, respectively. To isolate the ESA contribution dependent on the excitation wavelength, the difference spectrum is also plotted (grey line). The differential signal shows at 615 nm and 510 nm a distortion due to the excitation pulses.

This allows us to hypothesize that the molecule can access more configurations upon excitation of S_2 and S_3 than of S_1. The reason lies in the increased excess vibrational energy and the possible electronic relaxation pathways from S_2 and S_3, due to the coupling with even higher electronic states. Among these new accessible configurations, one (or more) is significantly different and rather stable (at least several ns). Accordingly, the photo-excited molecule can be considered a

photo-isomer of the initial one. Reaching different geometries depending on the excitation wavelength, could be referred to as anti-Kasha photochemistry,[8] and more specifically as anti-Kasha photo-isomerization. Figure 3 provides a graphic summary of the photocycle of (**1**), including, pictorially, the anti-Kasha photo-isomerization.

The anti-Kasha emission stems from a competition between the lifetimes of the radiative $S_2 \rightarrow GS$ relaxation channel (τ_{rad}) and the total lifetime of S_2 (τ_{Tot}), which is determined by the non-radiative $S_2 \rightarrow S_1$ IC process. Accordingly, since

$$\Phi = \frac{\tau_{Tot}}{\tau_{rad}}$$

the radiative lifetime should be 22 ns (=1.4ps/0.0064%), which is a reasonable value for a weakly allowed transition (Table S2) and consistent with the observed values.

Following the introductory notes about the determining role of a Quinoxdt ligand in the anti-Kasha emission[15–17] and the assignment of S_2 to a molecular orbital centered on the Quinoxdt ligand (Figure 1), it is straightforward to assign the anti-Kasha emission to electronic transitions mainly localized on this ligand. This is experimentally confirmed by the remarkable match of the PLE of (**1**) with the ones of other metal-Quinoxdt complexes (Figure S14 and Figure S15). TD-DFT calculations on the equilibrated second excited state corroborate the observed anti-Kasha emission at 720 nm and explain the lack of any observed emission from S_1 (Table S3 and relative discussion). The comparison of the optimized structures of GS and the first two excited states (Figure S4) reveals major conformational changes involving the MBAdto counter-ligand, which are not expected in the other complexes (see Figure S15 and relative discussion in SI). Indeed, due to its open structure, MBAdto is much more flexible than ligands of the other complexes where substituents at the dithiolene moiety (C2S2) are inserted in a ring (Figure S14). This higher

flexibility on the one hand allows a deeper energy relaxation and therefore a greater Stokes shift; on the other hand, it permits the exploration of many more different conformational configurations, leading to long-lived conformers when relaxing from S_2 or S_3.

In this respect, the observed anti-Kasha photochemistry originates from a synergetic combination of Quinoxdt and MBAdto features. Indeed, the comparison of the PLE spectra with the OA spectrum reveals that the anti-Kasha emission is induced only upon excitation of electronic states localized on the Quinoxdt ligand. Excitation towards higher, but short-lived excited states, does not induce any anti-Kasha activity. This agrees with the fact that the Quinoxdt ligand not only provides emissive states, but also slows down the $S_2 \rightarrow S_1$ IC process long enough to allow the MBAdto counter-ligand to explore and to find a different long-lived structural configuration.

In conclusion, the investigated sample shows a rich and complex anti-Kasha behavior where both anti-Kasha-emission and anti-Kasha photochemistry are observed. The former stems from the capability of Quinoxdt ligands to give a CT character to $S_2 \rightarrow S_1$ internal conversion. This general mechanism can explain the recurrent anti-Kasha emission observed in several other metal-Quinoxdt complexes. The latter, conversely, seems to rely on the increased flexibility of the MBAdto counter-ligand, which makes long-lived configurational isomers accessible, facilitated by the exceptionally long S_2 lifetime.

These results can inspire strategies to induce anti-Kasha behavior in donor-metal-acceptor compounds and a way to control the lifetime of their higher excited states. On perspective, they could suggest routes to synthesize and conceive novel (supra-)molecular complexes with a multi-responsive behavior.

ASSOCIATED CONTENT

Supporting Information available: Material and methods (sample preparation, steady state measurements, computational methods, femtosecond transient absorption, data analysis); TD-DFT calculations, complete transient absorption experiments at 615 nm and 510; comparison with other dithiolene complexes (PDF). This information is available free of charge.

AUTHOR INFORMATION

The authors declare no competing financial interests.

ACKNOWLEDGMENT

M.G., A.C., E.R. and T.F. acknowledge the financial support from the Swiss NSF through the NCCR MUST "Molecular Ultrafast Science and Technology". A.C. was supported by Swiss NSF through the grant 200021_172696. P.D., L.P., S.S.A. thank Università di Cagliari for the support. F.A. acknowledges the Research Foundation Flanders and the EU Horizon 2020 program for a [PEGASUS]2 Marie Skłodowska-Curie grant (agreement No665501, project 12U3417N LV).

REFERENCES

(1) Kasha, B. Y. M. Characterization of Electronic Transitions in Complex Molecules. *Discuss. Faraday Soc.* **1950**, *9* (c), 14–19.

(2) Kasha, M.; McGlynn, S. P. Molecular Electronic Spectroscopy. *Annual Review of Physical Chemistry* **1956**, *7* (1), 403–424. https://doi.org/10.1146/annurev.pc.07.100156.002155.

(3) Viswanath, G.; Kasha, M. Confirmation of the Anomalous Fluorescence of Azulene. *The Journal of Chemical Physics* **1956**, *24* (3), 574–577. https://doi.org/10.1063/1.1742548.

(4) Itoh, T. Fluorescence and Phosphorescence from Higher Excited States of Organic Molecules. *Chemical Reviews* **2012**, *112* (8), 4541–4568. https://doi.org/10.1021/cr200166m.

(5) Klán, P.; Wirz, J. *Photochemistry of Organic Compounds: From Concepts to Practice*; John Wiley & Sons, 2009. https://doi.org/10.1002/9781444300017.

(6) Chang, Y. C.; Tang, K. C.; Pan, H. A.; Liu, S. H.; Koshevoy, I. O.; Karttunen, A. J.; Hung, W. Y.; Cheng, M. H.; Chou, P. T. Harnessing Fluorescence versus Phosphorescence Branching Ratio in (Phenyl)n-Bridged (n = 0-5) Bimetallic Au(I) Complexes. *Journal of Physical Chemistry C* **2013**, *117* (19), 9623–9632. https://doi.org/10.1021/jp402666r.

(7) Yeow, E. K. L.; Steer, R. P. Energy Transfer Involving Higher Electronic States: A New Direction for Molecular Logic Gates. *Chemical Physics Letters* **2003**, *377* (3–4), 391–398. https://doi.org/10.1016/S0009-2614(03)01150-3.

(8) Demchenko, A. P.; Tomin, V. I.; Chou, P. T. Breaking the Kasha Rule for More Efficient Photochemistry. *Chemical Reviews* **2017**, *117* (21), 13353–13381. https://doi.org/10.1021/acs.chemrev.7b00110.

(9) Shi, L.; Yan, C.; Guo, Z.; Chi, W.; Wei, J.; Liu, W.; Liu, X.; Tian, H.; Zhu, W. H. De Novo Strategy with Engineering Anti-Kasha/Kasha Fluorophores Enables Reliable Ratiometric Quantification of Biomolecules. *Nature Communications* **2020**, *11* (1), 1–11. https://doi.org/10.1038/s41467-020-14615-3.

(10) Myahkostupov, M.; Pagba, C. v; Gundlach, L.; Piotrowiak, P. Vibrational State Dependence of Interfacial Electron Transfer: Hot Electron Injection from the S1 State of Azulene into TiO2 Nanoparticles. *Journal of Physical Chemistry C* **2013**, *117* (40), 20485–20493. https://doi.org/10.1021/jp406662n.

(11) Becker, R. S.; Pelliccioli, A. P.; Romani, A.; Favaro, G. Vibronic Quantum Effects in Fluorescence and Photochemistry. Competition between Vibrational Relaxation and Photochemistry and Consequences for Photochemical Control. *Journal of the American Chemical Society* **1999**, *121* (10), 2104–2109. https://doi.org/10.1021/ja982933p.

(12) Nazari, M.; Bösch, C. D.; Rondi, A.; Francés-Monerris, A.; Marazzi, M.; Lognon, E.; Gazzetto, M.; Langenegger, S. M.; Häner, R.; Feurer, T.; Monari, A.; Cannizzo, A. Ultrafast Dynamics in Polycyclic Aromatic Hydrocarbons: The Key Case of Conical Intersections at Higher Excited States and Their Role in the Photophysics of Phenanthrene Monomer. *Physical Chemistry Chemical Physics* **2019**, *21* (31), 16981–16988. https://doi.org/10.1039/c9cp03147b.

(13) Niu, Y.; Peng, Q.; Deng, C.; Gao, X.; Shuai, Z. Theory of Excited State Decays and Optical Spectra: Application to Polyatomic Molecules. *Journal of Physical Chemistry A* **2010**, *114* (30), 7817–7831. https://doi.org/10.1021/jp101568f.

(14) Röhrs, M.; Escudero, D. Multiple Anti-Kasha Emissions in Transition-Metal Complexes. *Journal of Physical Chemistry Letters* **2019**, *10* (19), 5798–5804. https://doi.org/10.1021/acs.jpclett.9b02477.

(15) Attar, S.; Espa, D.; Artizzu, F.; Pilia, L.; Serpe, A.; Pizzotti, M.; di Carlo, G.; Marchiò, L.; Deplano, P. Optically Multiresponsive Heteroleptic Platinum-Dithiolene Complex with Proton Switchable Properties. *Inorganic Chemistry* **2017**, *56* (12), 6763–6767.

(16) Attar, S. S.; Artizzu, F.; Marchiò, L.; Espa, D.; Pilia, L.; Casula, M. F.; Serpe, A.; Pizzotti, M.; Orbelli-Biroli, A.; Deplano, P. Uncommon Optical Properties and Silver-Responsive Turn-Off/On Luminescence in a PtII Heteroleptic Dithiolene Complex. *Chemistry* **2018**, *24* (Chemistry A E), 1–11. https://doi.org/10.1002/chem.201801697.

(17) Attar, S.; Espa, D.; Artizzu, F.; Mercuri, M. L.; Serpe, A.; Sessini, E.; Concas, G.; Congiu, F.; Marchiò, L.; Deplano, P. A Platinum-Dithiolene Monoanionic Salt Exhibiting Multiproperties, Including Room-Temperature Proton-Dependent Solution Luminescence. *Inorganic Chemistry* **2016**, *55* (11), 5118–5126. https://doi.org/10.1021/acs.inorgchem.5b02491.

(18) Espa, D.; Pilia, L.; Makedonas, C.; Marchiò, L.; Mercuri, M. L.; Serpe, A.; Barsella, A.; Fort, A.; Mitsopoulou, C. A.; Deplano, P. Role of the Acceptor in Tuning the Properties of Metal [M(II) = Ni, Pd, Pt] Dithiolato/Dithione (Donor/Acceptor) Second-Order Nonlinear Chromophores: Combined Experimental and Theoretical Studies. *Inorganic Chemistry* **2014**, *53* (2), 1170–1183. https://doi.org/10.1021/ic402738b.

(19) Stiefel, E. I. *Dithiolene Chemistry: Synthesis, Properties, and Applications*, Progress i.; Karlin, K., Ed.; John Wiley & Sons, 2004.

(20) Frei, F.; Rondi, A.; Espa, D.; Mercuri, M. L.; Pilia, L.; Serpe, A.; Odeh, A.; van Mourik, F.; Chergui, M.; Feurer, T.; Deplano, P.; Vlček, A.; Cannizzo, A. Ultrafast Electronic and Vibrational Relaxations in Mixed-Ligand Dithione-Dithiolato Ni, Pd, and Pt Complexes. *Dalton transactions (Cambridge, England : 2003)* **2014**, *43* (47), 17666–17676. https://doi.org/10.1039/c4dt01955e.

(21) Lackowicz, J. R. *Principles of Fluorescence Spectroscopy*; Springer, 1984; Vol. 137. https://doi.org/10.1016/0003-2697(84)90125-8.

(22) Bixon, M.; Jortner, J.; Cortes, J.; Heitele, H.; Michel-Beyerle, M. E. Energy Gap Law for Nonradiative and Radiative Charge Transfer in Isolated and in Solvated Supermolecules. *Journal of Physical Chemistry* **1994**, *98* (30), 7289–7299. https://doi.org/10.1021/j100081a010.